05,08

Efficient current-induced magnetization reversal in metallic nanostructures

© A.V. Telegin, V.D. Bessonov, I.D. Lobov, V.S. Teplov

M.N. Mikheev Institute of Metal Physics, Ural Branch, Russian Academy of Sciences, Yekaterinburg, Russia

E-mail: telegin@imp.uran.ru

Received October 6, 2023
Revised October 6, 2023
Accepted October 7, 2023

Samples of metallic thin-film nanostructures consisting of ferromagnetic (FM) and heavy metal (HM) layers were fabricated using magnetron sputtering techniques, and current-carrying structures with locally enhanced current density were formed. The energy of perpendicular magnetic anisotropy and the current density required for magnetization reversal of the structures were determined from magnetic and transport measurements. Modeling of the specific resistance and current flowing through the nanostructure layers responsible for generating spin current was performed. It was shown that all samples exhibit a magnetic response to current flow due to the Hall spin effect. The specific current-induced field parameters and the efficiency of current-induced switching were determined for the obtained nanostructures, as well as their dependence on the type of HM and the thickness of the FM layer. The results of this work are of interest for studying transport effects in multilayer structures and developing methods for controlling spin textures to create new memory and computing devices.

Keywords: Magnetron sputtering, current-induced magnetization, Hall effect, spintronics, nanostuctures, spin current, Kerr microscopy.

DOI: 10.61011/PSS.2023.12.57689.221

1. Introduction

The development of technologies for processing large volumes of data, including artificial intelligence systems, requires a high-performance and energy-efficient element base. One of the promising directions in the development of modern electronics is spintronics, in which manipulations are performed not with the charge, but with the spin of the electron [1–3]. Fundamental studies at the intersection of topological magnetism and spintronics are associated with the formation in recent years of two new promising directions spin-orbitronics [4–6] and skyrmionics [7]. Current problems of spin-orbitronics include the study of the nature of topological magnetism in collinear and non-collinear spin systems with strong spin-orbit coupling and Dzyaloshinsky–Moriya interaction [8–11]. Researchers are intensively searching for optimal parameters and materials based on thin magnetic metal films, in which spontaneous or parametric nucleation of chiral spin textures skyrmions is possible [12–14]. Note that the traditional way of creating skyrmion structures is based on a thermodynamic approach: by varying the magnitude and sign of the Dzyaloshinsky–Moriya interaction (DMI), exchange interaction, magnetic anisotropy and magnetostatic interaction thermodynamic stability of the skyrmion state is achieved. Unlike static skyrmions, dynamic skyrmions have their own high-frequency dynamics, which makes them especially attractive for practical applications [14–17]. Studies of spin textures and their dynamic properties under the influence of spin-orbit effects in multilayer nanostructures contribute to the development of a new direction — dynamic spintronics. Dynamic magnetic skyrmions are nanoscale topologically nontrivial soliton objects that can be obtained in perpendicularly magnetized magnetic films by exposure to spin currents or magnetic/electric fields [18–20]. For this purpose, we can use the effect of spin-transfer torque (STT) directly in the magnetic layer, or the more energy-efficient effect of spin-orbit torque (SOT) transfer from the spin current arising in the non-magnetic layer of heavy 4d- or 5d-metal due to the Hall spin effect [21,22]. If in this case the magnitude and sign of the DMI corresponds to the thermodynamic stability of the skyrmion state, then this dynamic state will persist even after the stimulating effect switching out. As was shown in [21], skyrmions can be induced, for example, by Oersted fields created by electric currents, which are responsible for the necessary inversion asymmetry [23]. The external magnetic field exclusion from the skyrmion control circuit makes it possible to implement a fully electrically controlled skyrmion memory [24]. However, the introduction of memory devices based on skyrmions is prevented, on the one hand, by the lack of data on the parameters of topological states and the lack of reliable methods for the generation and control of the dynamics and sizes of skyrmions; on the other hand, it is not yet completely clear which materials or structures are most suitable for these purposes at room temperature.

Among the promising materials that can contribute to this important problem solution, thin metal films and nanoheterostructures are attractive. This is due to their

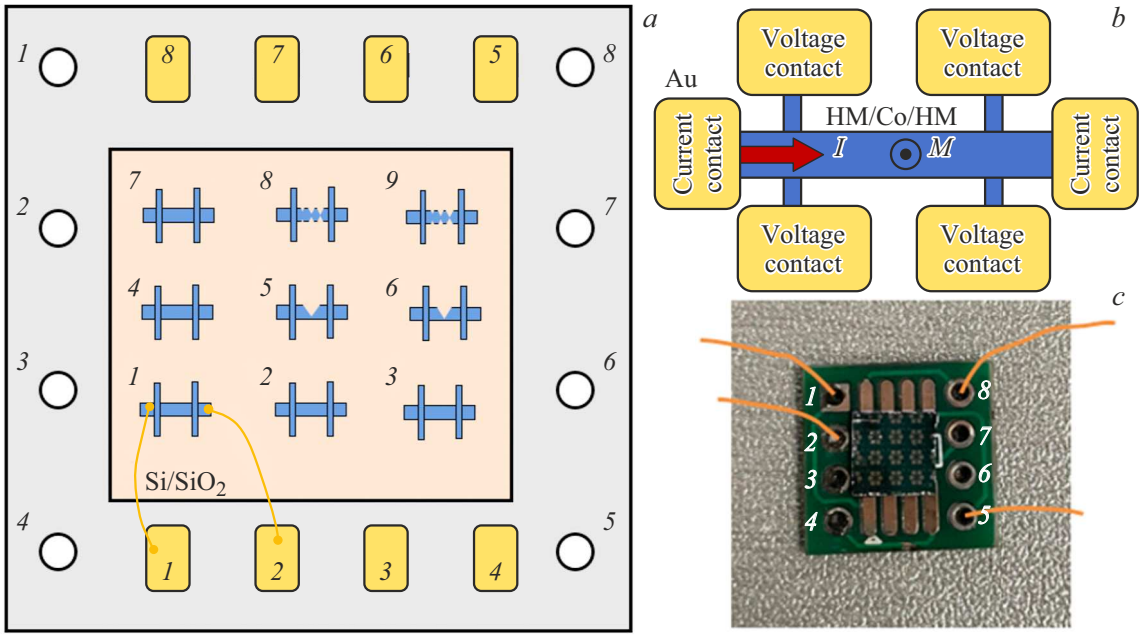

Figure 1. *a*) Diagram of Hall structures location on the sample relative to the chip contacts. *b*) Hall structure diagram with six contacts for a multilayer sample of HM (heavy metal)|Co|HM type. *c*) Photograph of the finished sample on the chip.

wide functionality under normal conditions, thanks to the combination of magnetic and non-magnetic layers, control of their size, geometry and quality of interfaces. The presence of strong DMI in nanostructures of the heavy metal|ferromagnetic type with perpendicular magnetic anisotropy (PMA) [25–28] made it possible to significantly expand the range of experimental systems and conditions in which topological magnetic structures can be observed. Studies in recent years shown that ferrimagnetics have greater potential for solving these problems than ferromagnetics, which determine the stability and minimum size of spin textures, speed, energy efficiency, etc. [29–31]. Therefore, important tasks for the development of spin-orbitronics and skyrmionics are: studying the dependence of the magnetic properties of nanostructures on the structure and type of layers and interfaces, and identifying effective ways to control the magnetic parameters of both ferro- and ferrimagnetic metal nanostructures with strong DMI.

In this paper, ferro- and ferrimagnetic nanostructures with Co were synthesized, and their magnetic and magnetotransport properties were studied. It is shown that all samples have a domain structure and a magnetic response to the transmittance of current due to the Hall spin effect. The nature of the response strongly depends on the parameters of the structure layers. The maximum efficiency of current-induced remagnetization is observed for the CoTb ferrimagnetic layer. In this case, the magnetization switching current density was about 10^{11} A/m^2. It is assumed that current-induced effects can be effectively used for dynamic monitoring and control of spin textures in metal nanostructures.

2. Methods for obtaining and certifying samples

Multilayer films of composition
Ru(10)|Co(0.8)|Ru(2)−Ru|Co,
Ru(10)|Co(0.8)|Ru(2)|W(4)−Ru|Co|W,
W(4)|$Tb_{30}Co_{70}$(6)|Ru(2)−TbCo|Ru,
W(4)|[Tb(0.6)|Co(1.4)]$_3$|Ru(2)−Tb|Co|Ru
and Pt(5)|Co(0.8)|MgO(2)|Pt(2)−Pt5|Co,
Pt(15)|Co(0.8)|MgO(2)|Pt(2)−Pt15|Co
(layer thicknesses are given in nm), were obtained on thermally oxidized silicon substrates using Omicron ultra-high vacuum complex, at a pressure of Ar 0.4 Pa. The sputtering rate was calibrated using NTEGRA Aura atomic-force microscope (AFM). The mean-square surface roughness was about three angstroms. Using a D8 Advance X-ray diffractometer, it was established that the resulting samples of the composition Pt−Co, Ru−Co are polycrystalline, and CoTb−Ru — amorphous.

A layer of photoresist was applied to individual films, from which a stencil of Hall structures with a current guide length of 200 and width of 20 μm was formed by electron beam lithography using Scios 2 DualBeam scanning electron microscope (Figure 1). To create templates for electrical contacts, a contact photolithography unit was used. Ti−Au layer about 60 nm thick was thermally deposited onto the contacts.

To study the features of spin dynamics in metal nanostructures associated with local increase in direct current density, structures of three types were formed on samples with Hall-type contacts (Figure 2). First type: constant

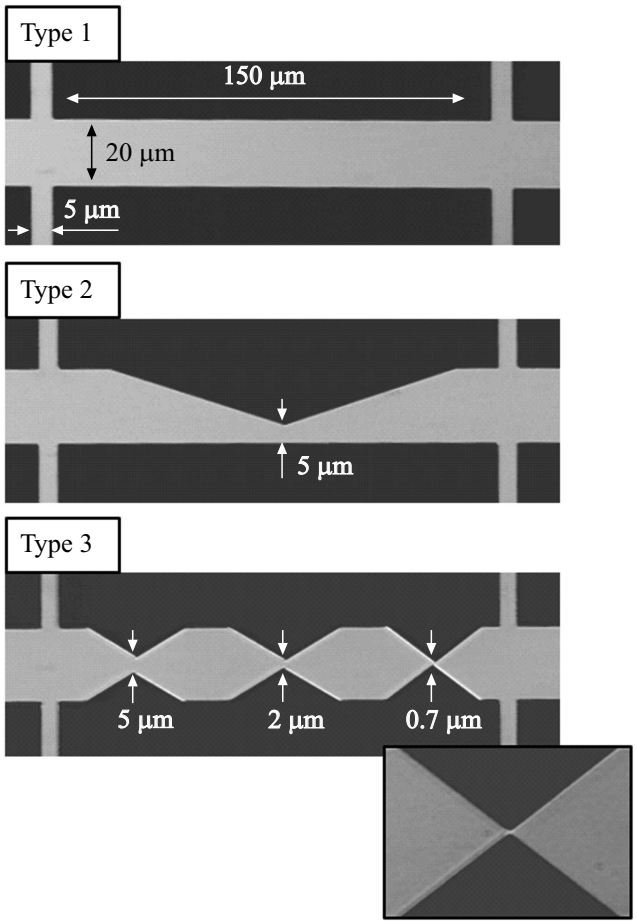

Figure 2. Three types of conductive Hall structures on film samples with different width of the conductive part.

thickness of the current conductive part — 20 μm. Second type: the current conductor on both sides narrows towards the center to width of 5 μm to create a current density gradient. Third type: three narrowings 5, 2 and 0.7 μm are created on the current conductor to achieve maximum current densities.

The final samples of film structures with size 4×4 mm, were placed on a silicon chip and welded using ultrasonic welding using the „wedge–wedge" method using aluminum wire with a diameter of 20 μm. Thus, there are 9 Hall structures on one sample on the chip: 5 structures of the first type, 2 structures of the second type, and 2 structures of the third type. Each Hall structure has six contacts: 2 at the edges of the current conductor and 4 transverse, for measuring the longitudinal and transverse potential difference when passing current.

The electrophysical properties were studied on two types of obtained samples: solid films and microtextured films with contacts. To connect to the chip pins, thin copper wires were soldered. The magnetic properties of the samples (saturation magnetization, coercive force, magnetic anisotropy energy, etc.) were studied on continuous films using LakeShore 7401 VSM vibration magnetometer. To determine the dynamics of remagnetization and to estimate the size of domains in samples of solid films and films with contacts, data from Kerr microscope Evico Magnetics were used. A quantitative assessment of the current effect on the magnetic structure of the sample was carried out at the original probe station.

3. Results and discussion

3.1. Magnetic and magneto-optical data

Experimental data of measurements of the field dependence of magnetization M for samples № 1–6 are presented in Figure 3. For all samples a typical magnetic hysteresis loop with the easy magnetization axis perpendicular to the film was obtained. A close to rectangular and narrow loop was obtained for structures with rare earth ions of terbium and cobalt, which have a hexagonal structure with easy magnetization axis along the axis c. Based on magnetization measurement data in fields of different orientations, the magnetic parameters of each sample were calculated: saturation magnetization and coercive force, energy and magnetic anisotropy field (see Table).

Figure 4 shows the features of the magnetic domain structure of continuous films and the Hall structure in demagnetized state and under the influence of the magnetic field or current for samples of nanostructures obtained from Kerr microscope.

3.2. Electric measurements

The electrical resistivity of the nanostructures under study was about $10^{-6}\,\Omega \cdot$ cm. As was shown, for example, in [32–34], passing the direct current in metal nanostructures leads to the induction of the effective magnetic field in the ferromagnetic (FM) layer due to the Hall spin effect, which occurs in the heavy metal (HM) layer.

However, in multilayer structures with a given configuration of electrical contacts, current flows not only through the HM layer, but also through the FM and auxiliary layers. Accordingly, to assess the efficiency of current-induced remagnetization reversal in the multilayer conducting nanostructure, we estimated the fraction of current p_i passing through the HM layer in the model of parallel resistors

$$p_i = \frac{h_i}{\rho_i} \frac{1}{\Sigma_i \frac{h_i}{p_i}} \cdot 100\%,$$

where t_i — thickness of i-th layer, ρ_i — resistivity of the layer with thickness h_i.

Figure 5 shows the calculation equivalent circuits of the electrical resistance of multilayer structures for each composition. The percentage of the current passing through each layer of the structure is indicated. It can be seen that for all types of structures about 90–95% of current flows through the HM layers. In this case, the share of HM main

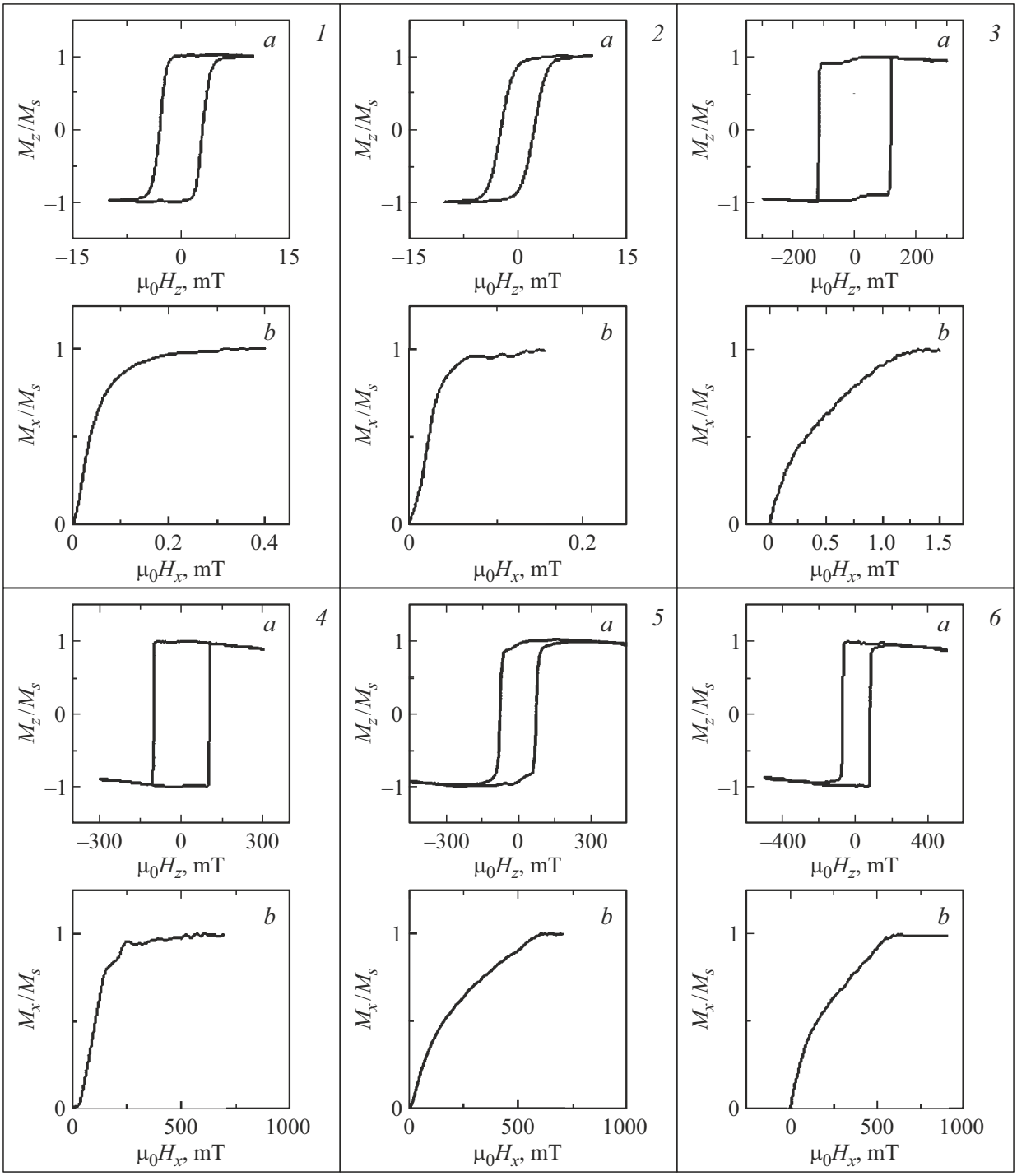

Figure 3. Field dependences of the relative magnitude of the magnetization component in external field directed *a*) perpendicular and *b*) parallel to the plane of the samples: *1* — Ru|Co, *2* — Ru|Co|W, *3* — TbCo|Ru, *4* — Tb|Co|Ru, *5* — Pt5|Co, *6* — Pt15|Co.

lower layer, i.e. the current efficiency of such multilayer structure is more than 50%.

Studying the behavior of magnetization in nanostructures when passing current with the help of Kerr microscope (Figure 4) made it possible to determine the magnitude of the current I_c at which magnetization switching occurs, and the switching current density. Having determined the resistance of samples with Hall structure, the dimensions of the current-conducting part and knowing the composition, we calculated the resistivity and the fraction of current passing through the layer inducing the spin-polarized current. The current efficiency values shown in Figure 5 are calculated using the example of type 1 structures, where the current density is the same along the entire length of the current

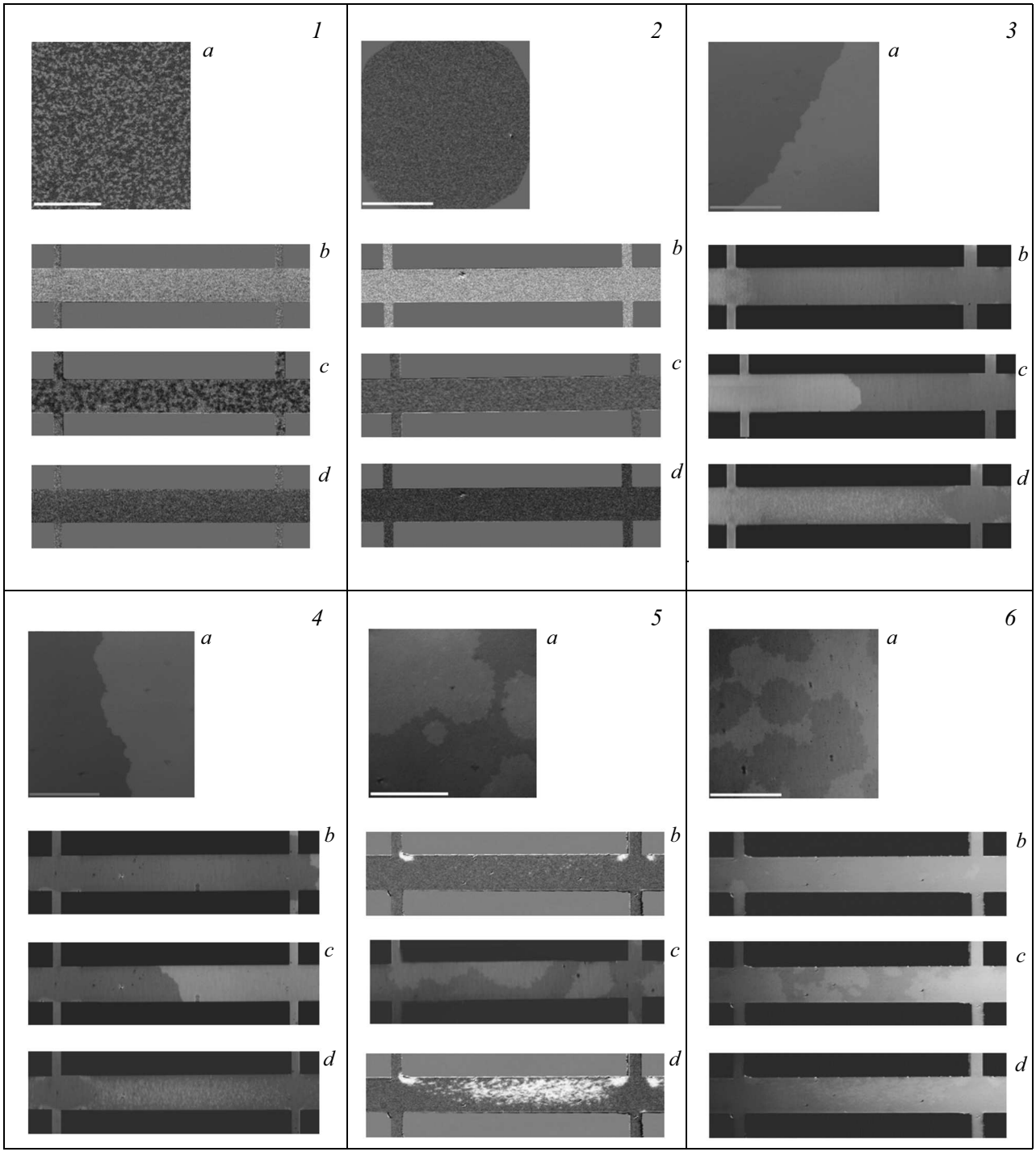

Figure 4. Visualization using Kerr microscope of remagnetization processes: *a*) demagnetized films, *b*) films under the influence of field, *c*) Hall structures under the influence of the field, and *d*) Hall structures under the influence of current, for samples: *1* — Ru|Co, *2* — Ru|Co|W, *3* — TbCo|Ru, *4* — Tb|Co|Ru, *5* — Pt5|Co, *6* — Pt15|Co.

conductor. In structures of the second and third types the change in the cross-section area leads to a multiple increase in the current density in the HM layer. As an example, Figure 6 shows the results of visualization of the current density distribution in inhomogeneous structures of types 2 and 3, obtained during computer simulation. For CoTb structures the minimum observed switching current density was $\sim 10^{11}\,\mathrm{A/m^2}$ (at a critical current value 20–40 mA), which is close to the previously observed minimum value — $\sim 2.5 \cdot 10^{10}\,\mathrm{A/m^2}$ [35]. The maximum observed value of the motion speed of the domain wall under the influence of current was $\sim 10\,\mu$m/s.

Magnetic and electrical characteristics of the obtained samples of nanostructures

Sample composition	*1*_Ru|Co|Ru	*2*_Ru|Co|Ru|W	*3*_W|Tb30Co70|Ru	*4*_W|[Tb|Co]3|Ru	*5*_Pt|Co|MgO|Pt	*6*_Pt|Co|MgO|Pt
Saturation magnetization M_s, 10^6 A/m)	0.51	0.49	0.21	0.25	0.80	0.87
Anisotropy field H_a, mT	450	150	900	510	600	590
Energy of magnetic anisotropy K_u, 10^5 J/m^3	0.43	0.13	0.9	0.30	1.67	1.77
Coercive force H_C, mT	2.9	2.2	116.5	102.3	74	75
Switching current I_c, mA	–	48	31	27	40	38
Density of switching current j_c, 10^{11} A/m^2)	–	1.4	1.3	1.1	2.6	1
Current share through HM p, %	77	29	68	68	55	79
Resistivity ρ, $10^{-6}\ \Omega \cdot$ m	0.51	1.2	1.7	1.8	0.47	0.46
Specific current-induced field β, 10^{-3} T/A	12	36	208	232	166	160
Efficiency of current-induced remagnetization ξ	0.09	0.11	1.82	1.4	0.32	0.4

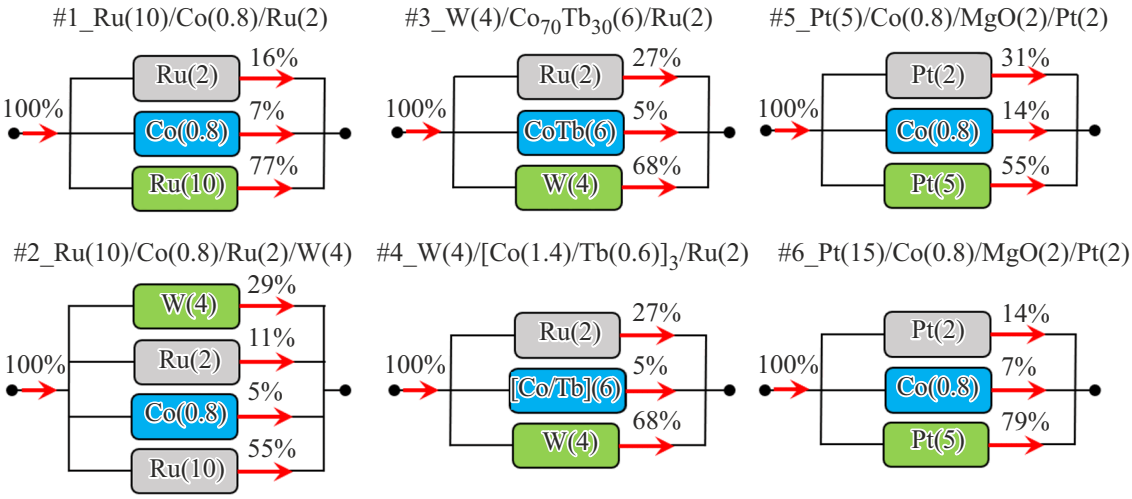

Figure 5. Resistance diagrams of multilayer structures of different compositions. The percentage of the current passing through the layer is indicated.

To assess the efficiency of current-induced remagnetization of nanostructures, the transverse potential difference was recorded when current was passed, using Hall structures obtained on samples. The potential difference arises due to the anomalous Hall effect (AHE) [22,33], and its value is proportional to the perpendicular component of the magnetization. A change in the external perpendicular magnetic field leads to remagnetization of the structure, which is reflected in the magnitude and field dependence of the AHE signal, which demonstrates a rectangular hysteresis loop (Figure 7).

When current is passed through the samples, due to the Hall spin effect, a spin-polarized current will be injected into the FM layer, which will cause additional rotation of the magnetic moments. For a certain direction of this rotation, it is possible to change the symmetry of the effect by turning on the constant magnetic field in the plane of the sample — a standard scheme for implementing remagnetization as a result of the transfer of spin magnetic moment. It is assumed that in this case the current will induce the additional field — B^z_{SOT} (Figure 7), perpendicular to the sample plane, and the hysteresis loop will move to the left or right by this amount, depending on the direction of current transmittance (red and blue loop in Figure 7 and 8).

Study of the magnitude of this offset on the current strength in the samples revealed a linear dependence (Figure 8), which determines the coefficient of proportionality β between the current passed through the structure and the

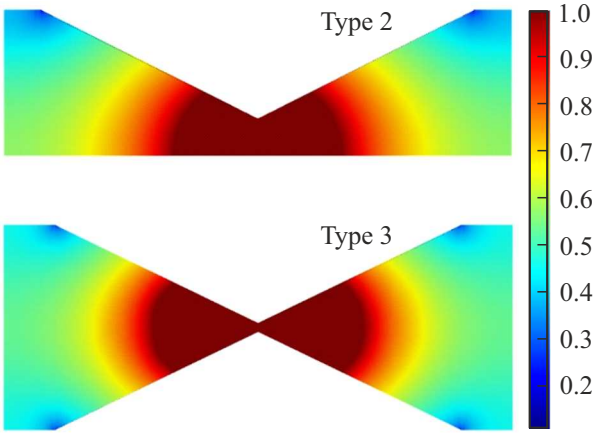

Figure 6. Current density distribution in structures of type *2* and *3* with jumper 2 and 0.7 μm.

field induced by it (in the presence of constant magnetic field in sample plane).

For each of the samples the dependences of the loops displacement on the value of the passed current were studied, and the coefficient β was determined. Based on the scheme in Figure 7, *b*, the illustrated offset of loops is due to the perpendicular component of the field B^z_{SOT} only. To determine the full value, it is necessary to take into account that B_{SOT} is oriented perpendicular to the magnetization. Then, knowing the anisotropy field, which keeps the magnetization perpendicular to the plane, and the magnitude of the external field in the plane we can determine the angle of inclination of the magnetization and the value B_{SOT} using the formula

$$B_{\mathrm{SOT}} = \frac{B^z_{\mathrm{SOT}}}{\sin\left(\mathrm{arctn}\left(B_x/B_a\right)\right)}. \qquad (1)$$

Based on the values of the coefficients β, B^z_{SOT}, magnetization saturation $\mathbf{M}_s$ and field $\mathbf{M}_x$ of anisotropy the efficiency of current-induced remagnetization was calculated using the formula [4]:

$$\xi = \frac{2e}{\hbar} M_S t_F \frac{B_{\mathrm{SOT}}}{j}, \qquad (2)$$

where e — electron charge, $\hbar$ — reduced Planck's constant, t_F — thickness of the magnetic layer, j — density of current flowing through the structure, B_{SOT} — current-induced field.

The obtained values of the specific current-induced field β and the efficiency of current-induced remagnetization ξ for each of the samples are given in the Table. Further, they can be used to evaluate the efficiency of spin transport in metal multilayer structures.

Structures based on Pt–Co with MgO interlayer demonstrate high efficiency of spin transport and are the most studied for problems of current-induced, including ultrafast remagnetization, and can be used to test the method used. In [36,37] it was shown that in the Ru|Co|Ru structure the magnitude of the current-induced remagnetization is negligible, since the Ru layer almost does not induce the spin-polarized current. The actual current passed through the sample affects the magnetic structure only through Joule heating and the induced Oersted field, while spin moment transfer cannot induce magnetization switching. Thus, such a structure can only be used as a reference when studying the influence of indirect exchange interaction on spin dynamics and various spin-dependent scattering processes in nanostructures. Note that adding W layer as HM leads to increase in the efficiency of magnetization switching by several times, with a constant thickness of FM layer, which is consistent, for example, with the data in [38].

Samples with Tb are ferrimagnetic, the magnetic moment of which depends on the mutual concentration of atoms. In [39,40] and other papers it was shown that with change in the thickness of the ferrimagnetic layer CoTb it is possible to transit between saturation states at a fixed composition. However, the maximum efficiency of the current-induced effect is observed in the vicinity of the ferrimagnetic compensation state, which can vary by changing the composition or thickness of the ferrimagnetic layer. In this case, the minimum switching current will correspond to the case

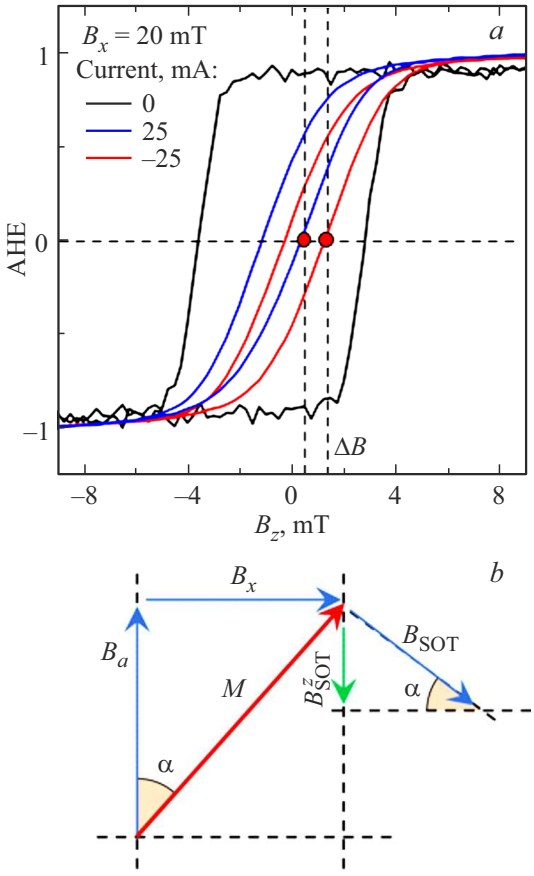

Figure 7. *a*) AHE hysteresis loops for nanostructure depending on the magnitude and orientation of the transmitted current; *b*) Scheme of the mutual orientation of external field B_x, effective fields of anisotropy B_a and magnetization M

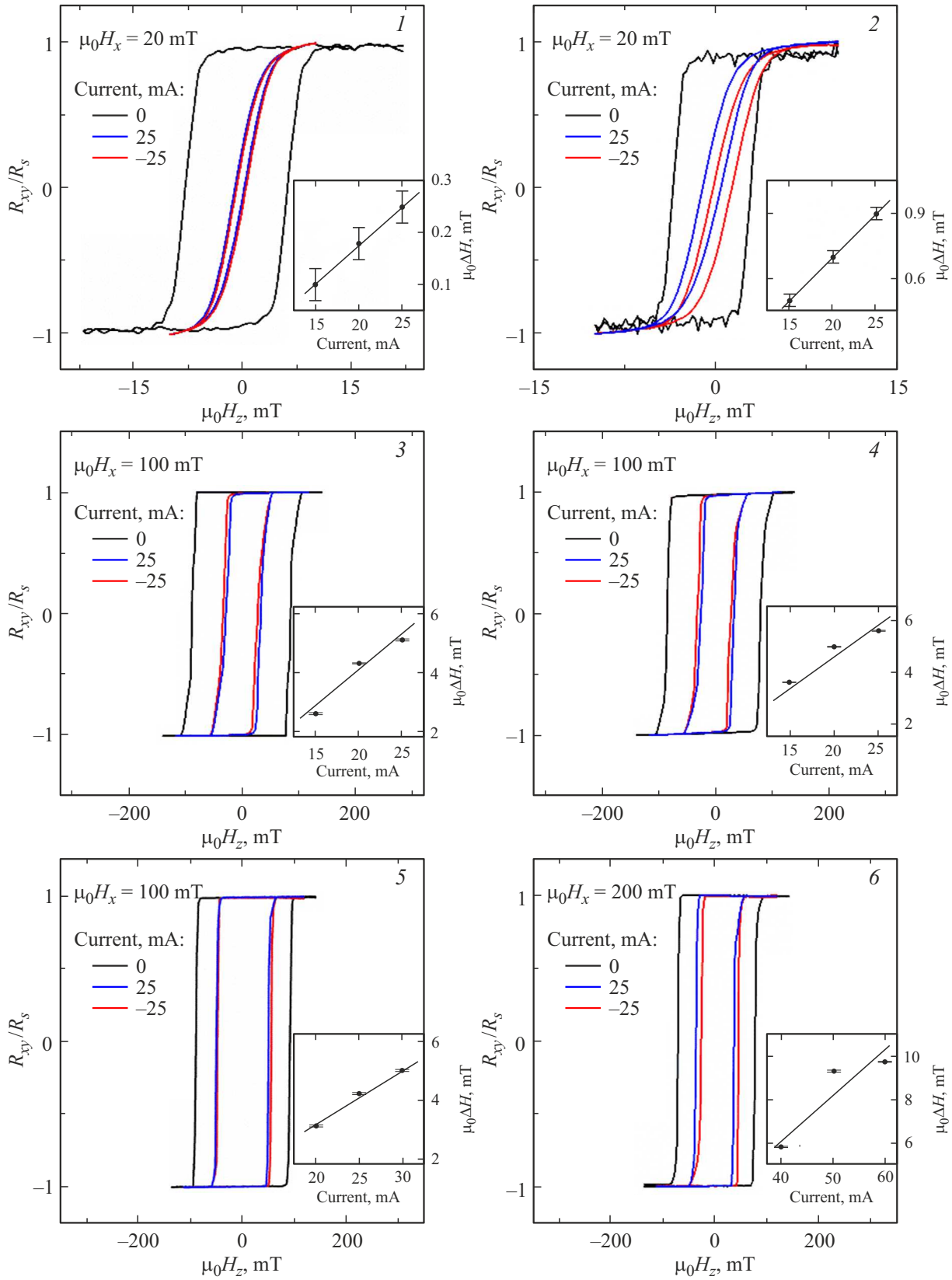

Figure 8. Hysteresis loops of the anomalous Hall effect R_x/R_s depending on the magnitude and orientation of the transmitted current in the samples: *1* — Ru|Co, *2* — Ru|Co|W, *3* — TbCo|Ru, *4* — Tb|Co|Ru, *5* — Pt5|Co, *6* — Pt15|Co. Inserts show the dependence of the current-induced field $\mu_0\Delta H$ on the current passed through the Hall structure.

of the minimum thickness of the ferrimagnetic layer and the minimum Co content in it, which is associated with the Joule heating effect. Therefore, for studies a structure with ion ratio about 70 : 30 was taken. At this ratio, the saturation magnetization of the sample was $0.2 \cdot 10^6$, whereas a Co monolayer of the same thickness would have saturation magnetization $1.2 \cdot 10^6$. Unlike nanostructures based on Pt−Co and Ru−Co, which have noticeable surface-induced perpendicular magnetic anisotropy, CoTb layer has a bulk anisotropy nature. This feature makes it possible to study magnetic layers of arbitrary thickness. If in structures based on Pt and Ru the thickness of Co was limited to 1 nm, then in ferrimagnetic CoTb samples the thickness of the magnetic layer was chosen to be 6 nm to ensure a higher level of response in magnetic and resonance study methods. The samples with Tb differ from each other in the structure of the magnetic layer: in the first case CoTb is alloy formed by simultaneous sputtering of target with Co and Tb; in the second case, layer-by-layer sputtering of Co(1.4 nm) and Tb(0.6 nm) was implemented. The resulting difference in the magnetic and spin-transport properties of these samples can be associated, first of all, with the presence of a larger number of interfaces and defects in the alloy than in the layered sample [39]. Note that the presence of larger number of interfaces can lead to increase in the interface contribution to the Dzyaloshinsky−Moriya interaction similarly to alloys Pt−Co [27], the estimate of which is beyond scope of this paper.

4. Conclusion

Using magnetron sputtering, on substrates made of dioxide silicon) the polycrystalline films of multilayer nanostructures Ru(10)|Co(0,8)|Ru(2), Ru(10)|Co(0,8)|Ru(2)|W(4), W(4)|$Tb_{30}Co_{70}$(6)|Ru(2), W(4)|[Tb(0,6)|Co(1,4)]3|Ru(2), Pt(5)|Co(0,8)|MgO(2)|Pt(2), Pt(15)|Co(0,8)|MgO(2)|Pt(2) were synthesized. Using lithographic methods, Hall contact structures were obtained, and the magnetic and magnetotransport properties of nanostructures were studied. It was found that in all samples the effect of current-induced influence on the magnetic structure of the FM layer is observed, but the effectiveness of this influence can vary by almost two orders of magnitude depending on the TM layer. The maximum values of the specific current-induced field and the efficiency of current-induced remagnetization were obtained in ferrimagnetic alloys W(4)|$Tb_{30}Co_{70}$(6)|Ru(2), W(4)|$[Tb(0.6)|Co(1.4)]_3$|Ru(2), which can be recommended for further study of the processes of spin transport and current-induced remagnetization using optical and magneto-optical methods, including in method of pumping−probing. The influence of current-induced effects on the spin texture of thin-film metal nanostructures of the HM|FM type can be used in spin-electronic devices.

Acknowledgments

The authors express their gratitude for the assistance in measurements and synthesis of samples from the FEFU Center for Shared Use.

Funding

The work was supported by the Russian Science Foundation grant No. 21-72-20160 (https://rscf.ru/en/project/21-72-20160).

Conflict of interest

The authors declare that they have no conflict of interest.

References

[1] A. Fert. UFN **178**, *12*, 1336 (2008). (in Russian) https://doi.org/10.3367/UFNr.0178.200812f.1336
[2] Yu.K. Fetisov, A.S. Sigov, Radioelektronika. Nanosistemy. Informatsionnyie tekhnolgii **10**, *3*, 343 (2018). (in Russian).
[3] A.V. Ognev, A.S. Samardak. Vestn. DO RAN **4**, (128). 70 (2006). (in Russian)
[4] A. Manchon, J. Železný, I.M. Miron, T. Jungwirth, J. Sinova, A. Thiaville, K. Garello, P. Gambardella. Rev. Mod. Phys. **91**, *3*, 035004 (2019). https://doi.org/10.1103/RevModPhys.91.035004
[5] V.V. Ustinov, I.A. Yasyulevich, N.G. Bebenin. Phys. Met. Metallography **124**, *2*, 195 (2023).
[6] A.A. Stashkevich. J. Russ. Univ. Radioelectron. **22**, *6*, 45 (2019).
[7] A. Fert, N. Reyren, V. Cros. Nature Rev. Mater. **2**, *7*, 17031 (2017). https://doi.org/10.1038/natrevmats.2017.31
[8] I. Dzyaloshinsky. Sov. Phys. JETP **5**, *6*, 1259 (1957); J. Phys. Chem. Solids **4**, *4*, 241 (1958).
[9] T. Moriya. Phys. Rev. Lett. **4**, *5*, 228 (1960); Phys. Rev. **120**, *1*, 91 (1960).
[10] A.N. Bogdanov, U.K. Rößler. Phys. Rev. Lett. **87**, *3*, 037203 (2001). https://doi.org/10.1103/PhysRevLett.87.037203
[11] R.E. Camley, K.L. Livesey. Surface Sci. Rep. **78**, *3*, 100605 (2023). https://doi.org/10.1016/j.surfrep.2023.100605
[12] A. Fert, F.N. Van Dau. Comptes Rendus Phys. **20**, *7−8*, 817 (2019). https://doi.org/10.1016/j.crhy.2019.05.020
[13] A.N. Bogdanov, C. Panagopoulos. Nature Rev. Phys. **2**, *9*, 492 (2020). https://doi.org/10.1038/s42254-020-0203-7
[14] N. Nagaosa, Y. Tokura. Nature Nanotechnol. **8**, *12*, 899 (2013). https://doi.org/10.1038/nnano.2013.243
[15] K. Everschor-Sitte, J. Masell, R.M. Reeve, M. Kläui. J. Appl. Phys. **124**, *24*, 240901 (2018). https://doi.org/10.1063/1.5048972
[16] X. Zhang, Y. Zhou, K.M. Song, T.E. Park, J. Xia, M. Ezawa, S. Woo. J. Phys.: Condens. Matter **32**, *14*, 143001 (2020). https://doi.org/10.1088/1361-648X/ab5488
[17] B. Kaviraj, J. Sinha. ECS J. Solid State Sci. Technol. **11**, *11*, 115003 (2022). https://doi.org/10.1149/2162-8777/ac9eda
[18] J. Ding, X. Yang, T. Zhu. J. Phys. D **48**, *11*, 115004 (2015). https://doi.org/10.1088/0022-3727/48/11/115004
[19] F. Kammerbauer, F. Freimuth, R. Frö mter, Y. Mokrousov, M. Klä ui. J. Phys. Soc. Jpn **92**, *8*, 081007 (2023). https://doi.org/10.7566/JPSJ.92.081007

[20] W. Jiang, G. Chen, K. Liu, J. Zang, S.G.E. Te Velthuis, A. Hoffmann. Phys. Rep. **704**, 1 (2017). https://doi.org/10.1016/j.physrep.2017.08.00
[21] Y. Zhou, E. Iacocca, A.A. Awad, R.K. Dumas, F.C. Zhang, H.B. Braun, J. Åkerman. Nature Commun. **6**, *1*, 8193 (2015). https://doi.org/10.1038/ncomms9193
[22] J. Sinova, S.O. Valenzuela, J. Wunderlich, C.H. Back, T. Jungwirth. Rev. Mod. Phys. **87**, *4*, 1213 (2015). https://doi.org/10.1103/RevModPhys.87.1213
[23] O. Heinonen, W. Jiang, H. Somaily, S.G.E. Te Velthuis, A. Hoffmann. Phys. Rev. B **93**, *9*, 094407 (2016). https://doi.org/10.1103/PhysRevB.93.094407
[24] B. Paikaray, M. Kuchibhotla, A. Haldar, C. Murapaka. Nanotechnol. **34**, *22*, 225202 (2023). https://doi.org/10.1088/1361-6528/acbeb3
[25] A.I. Bezverkhnii, V.A. Gubanov, A.V. Sadovnikov, R.B. Morgunov. Phys. Solid State **63**, *12*, 2285 (2021).
[26] H. Yang, A. Thiaville, S. Rohart, A. Fert, M. Chshiev. Phys. Rev. Lett. **115**, *26*, 267210 (2015). https://doi.org/10.1103/PhysRevLett.115.267210
[27] J. Park, T. Kim, G.W. Kim, V. Bessonov, A. Telegin, I.G. Iliushin, A.A. Pervishko, D. Yudin, A.Yu. Samardak, A.V. Ognev, J. Cho, A.S. Samardak, Y.K. Kim. Acta Materialia **241**, 118383 (2022). https://doi.org/10.1016/j.actamat.2022.118383
[28] A.S. Samardak, A.G. Kolesnikov, A.V. Davydenko, M.E. Steblii, A.V. Ognev. Phys. Met. Metallogr. **123**, *3*, 238 (2022). https://doi.org/10.1134/S0031918X22030097
[29] B.A. Ivanov. Fizika nizkikh temperatur **45**, *S9*, 1095 (2019). (in Russian).
[30] Y. Zhang, X. Feng, Z. Zheng, Z. Zhang, K. Lin, X. Sun, G. Wang, J. Wang, J. Wei, P. Vallobra, Y. He, Z. Wang, L. Chen, K. Zhang, Y. Xu, W. Zhao. Appl. Phys. Rev. **10**, 1 (2023). https://doi.org/10.1063/5.0104618
[31] S.K. Kim, G.S.D. Beach, K.-J. Lee T. Ono, T. Rasing, H. Yang. Nature Mater. **21**, *1*, 24 (2022). https://doi.org/10.1038/s41563-021-01139-4
[32] B. Divinskiy, V.E. Demidov, A. Kozhanov, A.B. Rinkevich, S.O. Demokritov, S. Urazhdin. Appl. Phys. Lett. **111**, *3*, 032405 (2017).
[33] A. Hoffmann. IEEE Trans. Magn. **49**, *10*, 5172 (2013). https://doi.org/10.1109/TMAG.2013.2262947
[34] V.E. Demidov, S. Urazhdin, R. Liu, B. Divinskiy, A. Telegin, S.O. Demokritov. Nature Commun. **7**, *1*, 10446 (2016). https://doi.org/10.1038/ncomms10446
[35] M.E. Stebliy, M.A. Bazrov, Z.Z. Namsaraev, M.E. Letushev, A.G. Kozlov, V.A. Antonov, E.V. Stebliy, A.V. Davydenko, A.V. Ognev, Y. Shiota, T. Ono, A.S. Samardak. ACS Appl. Mater. Interfaces **15**, *34*, 40792 (2023). https://doi.org/10.1021/acsami.3c08979
[36] A.G. Kolesnikov, M.E. Stebliy, A.V. Ognev, A.S. Samardak, A.N. Fedorets, V.S. Plotnikov, X. Han, L.A. Chebotkevich. J. Phys. D **49**, *42*, 425302 (2016). https://doi.org/10.1088/0022-3727/49/42/425302
[37] A.G. Kolesnikov, A.V. Ognev, M.E. Stebliy, L.A. Chebotkevich, A.V. Gerasimenko, A.S. Samardak. J. Magn. Magn. Mater. **454**, 78 (2018). https://doi.org/10.1016/j.jmmm.2018.01.056
[38] W.L. Yang, Z.R. Yan, Y.W. Xing, C. Cheng, C.Y. Guo, X.M. Luo, M.K. Zhao, G.Q. Yu, C.H. Wan, M.E. Stebliy, A.V. Ognev, A.S. Samardak, X.F. Han. Appl. Phys. Lett. **120**, *12*, 122402 (2022). https://doi.org/10.1063/5.0079400
[39] Z. Zhao, Z. Xie, Y. Sun, Y. Yang, Y. Cao, L. Liu, D. Pan, N. Lei, Z. Wei, J. Zhao, D. Wei. Phys. Rev. B **108**, *2*, 024429 (2023). https://doi.org/10.1103/PhysRevB.108.024429
[40] R.Q. Zhang, L.Y. Liao, X.Z. Chen, T. Xu, L. Cai, M.H. Guo, H. Bai, L. Sun, F.H. Xue, J. Su, X. Wang, C.H. Wan, H. Bai, Y.X. Song, R.Y. Chen, N. Chen, W.J. Jiang, X.F. Kou, J.W. Cai, H.Q. Wu, F. Pan, C. Song. Phys. Rev. B **101**, *21*, 214418 (2020). https://doi.org/10.1103/PhysRevB.101.214418

Translated by I.Mazurov